Heme-deficient metabolism and impaired cellular differentiation as an evolutionary trade-off for human infectivity in Trypanosoma brucei gambiense

Eva Horáková (horakova@paru.cas.cz)
Biology Centre
Laurence Lecordier
Université Libre de Bruxelles
Paula Cunha
Laboratory of Neurovascular Signaling, Department of Molecular Biology, Université libre de Bruxelles (ULB)
Roman Sobotka
Institute of Microbiology https://orcid.org/0000-0001-5909-3879
Piya Changmai
Biology Centre
Catharina Langedijk
Biology Centre
Jan Van Den Abbeele
Institute of Tropical Medicine
Benoit Vanhollebeke
Université https://orcid.org/0000-0002-0353-365X
Julius Lukes
Czech Academy of Sciences, Institute of Parasitology https://orcid.org/0000-0002-0578-6618

Article

Keywords: African trypanosomes, trypanosome haptoglobin-hemoglobin receptor, Trypanosoma brucei gambiense

Posted Date: September 8th, 2020

DOI: https://doi.org/10.21203/rs.3.rs-49796/v1

Additional Declarations: There is **NO** Competing Interest.

Version of Record: A version of this preprint was published at Nature Communications on November 18th, 2022. See the published version at https://doi.org/10.1038/s41467-022-34501-4.

Heme-deficient metabolism and impaired cellular differentiation as an evolutionary trade-off for human infectivity in *Trypanosoma brucei gambiense*

Eva Horáková[1,#,*], Laurence Lecordier[2,#], Paula Cunha[2,#,%], Roman Sobotka[3,4], Piya Changmai[1,§], Catharina J. M. Langedijk[1,&], Jan Van Den Abbeele[5], Benoit Vanhollebeke[2,6 &] Julius Lukeš[1,3,*]

[1] Institute of Parasitology, Biology Centre, Czech Academy of Sciences, České Budějovice (Budweis), Czech Republic

[2] Laboratory of Neurovascular Signaling, Department of Molecular Biology, Université libre de Bruxelles (ULB), Gosselies, Belgium

[3] Faculty of Sciences, University of South Bohemia, České Budějovice (Budweis), Czech Republic

[4] Institute of Microbiology, Czech Academy of Sciences, Třeboň, Czech Republic

[5] Unit of Veterinary Protozoology, Institute of Tropical Medicine, Antwerp, Belgium

[6] Walloon Excellence in Life Sciences and Biotechnology, Belgium

[§] Present address: Faculty of Science, University of Ostrava, Ostrava, Czech Republic

[&] Present address: Cancer Center Amsterdam UMC, VU. University Medical Center, Amsterdam, The Netherlands

[%] Present address: Escola Paulista de Medicina, Universidade Federal de São Paulo, São Paulo, Brazil

[#] These authors contributed equally to the work

[*] To whom correspondence should be addressed:

Eva Horáková - horakova@paru.cas.cz; Julius Lukeš - jula@paru.cas.cz

ABSTRACT

Resistance to African trypanosomes in humans relies on high affinity targeting of a trypanosome lytic factor 1 (TLF1) to trypanosome haptoglobin-hemoglobin receptor (HpHbR). While TLF1 avoidance by the inactivation of the HpHbR contributes to *Trypanosoma brucei gambiense* human infectivity, the evolutionary trade-off of this adaptation is unknown, as the physiological function of the receptor remains to be elucidated. Here we show that uptake of hemoglobin *via* HpHbR constitutes the sole heme import pathway in the bloodstream stage of the animal trypanosome *T. brucei brucei*. Both *T. b. gambiense* with inactive HpHbR, as well as a genetically engineered *T. b. brucei* HpHbR knock-out show only trace levels of intracellular heme and lack the downstream hemoprotein activities, thereby providing an extraordinary example of aerobic parasite proliferation in the absence of heme. We further show that HpHbR facilitates the developmental progression by inducing PAD-1 expression that is associated with the formation of cell cycle-arrested stumpy forms in *T. b. brucei*. Accordingly, *T. b. gambiense* was found to be poorly competent for slender-to-stumpy differentiation unless a functional HpHbR receptor derived from *T. b. brucei* was genetically restored. Altogether, we identify two HpHbR-dependent evolutionary trade-offs for *T. b. gambiense* human infectivity.

INTRODUCTION

Through the combination of human infections and livestock trypanosomiasis, the neglected tropical diseases caused by African trypanosomes belonging to *Trypanosoma brucei sensu lato* (*s.l.*) have a significant impact on sub-Saharan rural development. Two sub-species of *T. brucei* proliferate in humans: *T. brucei gambiense* is responsible for a chronic and slowly progressing human trypanosomiasis, while *Trypanosoma brucei rhodesiense* causes an acute form of the disease (1). When injected by the blood feeding insect vector (tsetse fly; *Glossina* spp.) into the human tissue, animal-infecting *T. brucei brucei* is rapidly killed by a potent arm of the innate immune system, represented by trypanosome lytic factors (TLF) 1 and 2 (2, 3). TLF1 is composed of haptoglobin-related protein (4) and apolipoprotein L-1 (5) and targets the parasites efficiently by engaging the haptoglobin-hemoglobin receptor (HpHbR), the only invariant cell surface receptor known to date in kinetoplastid parasites (6, 7).

The HpHb complex is formed by haptoglobin (Hp) and extracellular hemoglobin (Hb) resulting from intravascular hemolysis. The principal function of HpHbR, which was named after its only ligand, is heme uptake (6). Indeed, same as other trypanosomes, *T. brucei s.l.* are heme auxotrophs (8), who acquire external heme via HpHbR in the mammalian-infective bloodstream stage (BS) (6). The procyclic trypanosome stage (PS) in the tsetse fly midgut contains more hemoproteins and obtains the ancient and omnipresent heme cofactor using another dedicated transporter, *Tb*Hrg (9).

Nevertheless, HpHbR is not essential for the proliferation of BS since the monomorphic *T. b. brucei* knock-out for HpHbR (HpHbR KO) shows only a mildly affected growth phenotype *in vitro* (6, 10). Moreover, despite being more sensitive to the host's oxidative stress, this cell line kills its rodent host before the first wave of immunoglobulin-based immunity develops (6). Curiously, the capacity of *T. b. gambiense* to survive in human blood and cause infection is partially based on a point mutation in HpHbR that dramatically reduces its affinity for both TLF1 and HpHb (10, 11, 12, 13).

Retaining the HpHbR expression contribute to trypanosome's fitness in their animal reservoir hosts, providing positive selection pressures for the conservation of this receptor (6, 14). Still, it acquired critical mutations that allowed *T. b. gambiense* to enter a new niche, the human host, despite the attenuation in the primary animal hosts. The cost of this loss of HpHbR function was tolerable, although it brought a reduced capacity for cyclical transmission by the tsetse fly when compared with the closely related *T. b. brucei* and *T. b. rhodesiense*.

Here we confirm that *T. b. brucei* HpHbR KO does not uptake heme and newly demonstrate that it leads to the loss of the ability to fuel hemoproteins with this cofactor. Moreover, the loss of this receptor is associated with a reduced ability to undergo differentiation in the mammalian host. In the absence of HpHbR, the fast dividing long slender forms of the bloodstream stage (BS-SL) do not transform into the quiescent, transmission-competent stumpy forms of the bloodstream stage (BS-ST). As a natural mutant for HpHbR, the human pathogenic *T. b. gambiense* is poorly capable of importing heme and generating BS-ST, while both key features are restored by heterologous expression of the *T. b. brucei*-derived HpHbR.

RESULTS

Heme-free trypanosomes

T. brucei s.l. lost the capacity to synthesize heme and has to acquire it from its hosts (8). First, we verified previous fluorimetric measurements of heme amount (6) and showed consistent values from the mouse-collected BS parasites. Wild type (WT) *T. b. brucei* contains 100 pmol heme/10^9 cells, contrary to the *T. b. brucei* HpHbR KO cells, which exhibit only a trace amount of heme at the detection limit (Figs. 1A, B). For the first time, we established the amount of heme in WT *T. b. gambiense,* where also only a trace of heme was observed (6 pmol/10^9 cells), comparable to HpHbR KO cells (Figs. 1A, B).

Next, we studied how hemoproteins function under these conditions. Therefore, a V5-tagged human catalase (hCAT), a potent and widespread heme-dependent enzyme which is absent in the genome of *T. brucei s. l.* (15), was expressed in three cell lines, namely WT *T. b. brucei* and the derived HpHbR KO, and WT *T. b. gambiense* (Figs. 1C, D). This allowed us to follow the activity of exogenous hemoprotein, which showed a uniform distribution in the cytosol (Fig. 1E). The catalase activity was monitored *via* the production of molecular oxygen, forming visible bubbles in the cell suspension (Fig. 1F; inset) upon the addition of H_2O_2 as a substrate (Fig. 1C). This assay showed that catalase was active only in WT *T. b. brucei* (Fig. 1F), while it was inactive in both *T. b. brucei* HpHbR KO and *T. b. gambiense* (Fig. 1F). This result is best explainable by the failure of the latter trypanosomes to import heme due to the absence of a functional HpHbR. This experiment also demonstrated that when taken up by HpHbR, heme is delivered into the cytosol, where it is freely available for hemoproteins as a cofactor.

Endogenous hemoproteins activity depends on HpHbR

Being involved in the sterol metabolism (16, 17), the hemoprotein CYP51 is considered to be essential and, therefore, a promising drug target against different trypanosomatids (18, 19, 20). Ketoconazole is one of the broadly used compounds which binds to the active site of CYP51 and inhibits its activity (21). The genome of *T. brucei s.l.* encodes a single copy of CYP51, which is transcribed primarily in the PS and only weakly in the BS-SL and BS-ST cells (Fig. 2A). RNAi in the PS led to an efficient reduction of *CYP51* mRNA (Suppl. Fig. 1A) followed by almost complete elimination of the corresponding protein 5 days post-induction (Suppl. Figs. 1B), as also illustrated by reduced α-CYP51

immunostaining in the RNAi-induced cells (Suppl. Fig. 1C). The gradual loss of CYP51 was associated with a significant growth reduction of the PS cells (Suppl. Fig. 1D). Of note, we were unable to generate CYP51 KO cell lines in the PS suggesting its essentiality in the given stage.

In contrast to PS, CYP51 RNAi in the BS did not result in a significant growth alteration (Fig. 2B). However, the extent of mRNA down-regulation was not complete, leaving the basal level of expression (data not shown). Therefore, we generated CYP51 KO by homologous recombination of both alleles with hygromycin and phleomycin expression cassettes in the BS cells (Suppl. Fig. 1E). Again, the growth phenotype of the BS lacking CYP51 was only slightly affected, indicating that this protein is dispensable in this stage (Fig. 2C).

Next, we evaluated the sensitivity of CYP51 RNAi and KO cells to ketoconazole, a specific inhibitor of CYP51 (Figs. 2D, E). In agreement with the previously published IC_{50} values (22), there was no statistical difference between the parental WT and CYP51 KO cells (Fig. 2D). Still, concentrations of ketoconazole ranging from 2 to 8 µM affect the WT and CYP51 KO cells differentially, since the former cells reduced their growth rate, while the latter remained unaffected (note the biphasic behavior of the dose-response curve) (Fig. 2D; right panel). An identical effect was observed when the sensitivity to ketoconazole was followed in the CYP51 RNAi BS trypanosomes (Fig. 2D; left panel). Hence, CYP51 activity can be selectively inhibited with low doses of ketoconazole, discriminating between the cells with and without CYP51. In contrast, when higher doses of ketoconazole are applied, we do not see significant differences in the growth of WT and CYP51 mutant and the action of the drug should be assigned to the off-target effect.

HpHb uptake deficiency confers insensitivity to CYP51 inhibition

The pharmacological conditions described above allow assessing the activity of the hemoprotein CYP51 in the BS cells under the conditions of defective HpHb uptake. First, we exposed HpHbR KO cells to ketoconazole and showed they are insensitive to low doses of the drug (Fig. 2F), mimicking the phenotype observed for CYP51 RNAi and KO cells.

Next, the HpHbR pathway-dependent CYP51 activity readout was evaluated in the WT *T. b. rhodesiense* cells resistant to the lysis by the human serum independently of Hp-Hb uptake (23). Under different cultivation conditions, we modulate their access to the cognate ligand of the receptor. When grown in the Hp-containing human serum, in which the

heterodimeric HpHb ligand is formed, *T. b. rhodesiense* is sensitive to micromolar concentrations of ketoconazole (Fig. 2G). In contrast, when grown in the anhaptoglobinemic serum (24, 25), i.e. in the absence of Hp, cells exhibit reduced growth and become insensitive to the drug. Yet, complementation of the anhaptoglobinemic serum with purified human Hp reverted this phenotype (Fig. 2G), proving a positive correlation between the operational HpHb uptake and the CYP51 activity.

Combined, by indirect means, we showed the CYP51, as one of the genuine hemoproteins in trypanosomes is the downstream acceptor of the HpHb complex.

Artificial expression of HpHbR in stumpy forms does not interfere with life cycle progression

Due to RNA polymerase I-mediated polycistronic transcription, in trypanosomes, most regulation occurs post-transcriptionally (26). It was shown previously that the HpHbR expression is downregulated in the early phase of the BS-SL to BS-ST differentiation (27). We noticed that *HpHbR* and other genes involved in this interstagial switch are located at the very end of the polycistronic transcription units (data not shown). Therefore, we created a cell line (HpHbR-Luc), where the distance of *HpHbR* from the end of the polycistron was artificially increased by the insertion of a 10 kb-long *Luciferase* gene in front of the *procyclin* gene (Suppl. Fig. 2C). By following the expression of both *HpHbR* and *Luciferase* genes during *in vitro* differentiation, we detected that the *Luciferase* mRNA was continuously formed as judged by activity measurements (Fig. 3A). In contrast, the *HpHbR* mRNA was downregulated in HpHbR-Luc to the same extent as in the WT cells during the PS to BS differentiation (Fig. 3B). This data suggest that the distance from the end of the polycistronic unit is not a critical factor orchestrating the transcription efficiency during life cycle progression.

It is well known that 3' untranslated regions (UTRs) have a critical role in the regulation of transcripts stability in trypanosomes. We forced the expression of *HpHbR* in the BS-ST by fusing the *HpHbR* open reading frame to the 3' UTR of *PAD1* gene (Suppl. Fig. 2D), the product of which is exclusively expressed in the BS-ST (28). In this HpHbR-3'PAD1 cell line, the *HpHbR* expression is maintained until the *in vitro* differentiation reaches the PS, which expresses 5x more *HpHbR* mRNA when compared to the WT PS (Fig. 3C). The capacity of the HpHbR-3'PAD1 cell line to differentiate from the BS-SL to the BS-ST *in vivo* was evaluated in mice, where the typical parasitic wave characteristic for the WT trypanosomes

was produced (Fig. 3D). Moreover, *ex vivo* cells collected on day 4 were examined morphologically and the functionality of HpHbR was verified by the uptake of the fluorescently-labeled HpHb complex (Figs. 3E, F). As expected, the WT cells produced around 75% of the BS-ST cells, which were exclusively Hp-free. The HpHbR-3'PAD1 cells also retained the ability to form the BS-ST cells (~ 60% by day 4), all of which were Hp-positive due to the artificial expression of the receptor (Figs. 3E, F).

Since the ability of the HpHbR-3'PAD1 cell line to differentiate has been tested only in the mammalian host, we decided to also evaluate its capacity for transmission *via* tsetse flies. The midguts of flies fed with blood containing either the WT or HpHbR-3'PAD1 BS parasites were dissected after 10 days post-feeding, showing no significant difference in the infection rates (Fig. 3G). Next, we added reduced L-glutathione to the blood meal, which is known to enhance the trypanosome establishment in the tsetse midgut (29). Indeed, the infection rate reached up to 90%, but we did not observe a significant difference between the WT and HpHbR-3'PAD1 cells, and their ability to transform to the PS and establish the tsetse midgut infection (Fig. 3G). Altogether, these results show that trypanosomes with the prolonged expression of HpHbR still differentiate into the BS-ST and subsequent PS and retain the ability to infect tsetse flies.

T. b. brucei HpHbR KO does not produce stumpy forms

The BS trypanosomes undergo extensive cellular differentiation in preparation for an abrupt transmission from the mammalian blood into tsetse fly. As the intensity of infection increases through the rapid proliferation of the BS-SL cells, a parasite-derived stumpy induction factor accumulates, which promotes morphological transformation into the BS-ST (30).

In order to test whether heme and/or HpHbR play any role in this critical phase of the life cycle, the HpHbR KO has also been generated in the pleomorphic 90-13 *T. b. brucei* by replacing both alleles with the puromycin or phleomycin cassette (Suppl. Figs. 2A, B). Moreover, we have created an addback cell line, in which the HpHbR expression was restored from the 18S rRNA locus (18S AB), while in another cell line, a single HpHbR allele was restored *in situ* (*in situ* AB). First, the functionality of HpHbR in all tested cell lines was examined by fluorescence microscopy of Hp-labeled with a green fluorochrome (Hp-Alexa 488). As expected, the uptake of the HpHb complex was disrupted entirely in the HpHbR KO

cell line, while 80% of the WT cells were Hp-positive (Figs. 4A, B). Both above-described addback cell lines showed the re-establishment of the Hp uptake, although to a different extent. Overexpression of HpHbR from the 18S rRNA locus almost reached the WT values (70%), whereas only 20% of *in situ* AB cells were labeled (Figs. 4A, B).

Next, the capacity to undergo differentiation *in vitro* was analyzed by exposing the individual cell lines to *cis*-aconitate and a temperature decrease to 27 ^{o}C, which is known to trigger the BS to PS transformation. We followed their ability to proliferate and express the procyclin coat as a hallmark of the PS (Figs. 4C, D). Under these conditions, the majority of the WT cells (70%) became procyclin-positive by day 2 and reached high densities ($5x10^6$ cells/ml) by day 3 (Figs. 4C, D). In contrast, the HpHbR-KO cells differentiated into only a few PS cells that did not divide and eventually died out (Figs. 4C, D). Both AB cell lines showed a high capacity to differentiate *in vitro*, with 70% of cells covered by procyclin by day 2 (Fig. 4D), although the cell numbers were about half when compared to the WT (Fig. 4C).

Based on the *in vitro* data, we chose the *in situ* AB trypanosomes for further experiments, since their genetic background is more physiologically relevant compared to the bulky HpHbR expression from the 18S rRNA locus. The selected cell lines were analyzed for their capacity to differentiate *in vivo*. As shown in mice, the HpHbR KO cells initially proliferate somewhat slower as compared with the WT. However, on day 6 the infection rapidly accelerated, achieving a high parasitemia of ~3 x 10^8 cells/ml, leading to the termination of the experiment on the following day (Fig. 4E). In contrast, the WT (90-13) parasitemia declined on day 6, while the *in situ* AB cells went halfway, reaching a plateau on day 7 (Fig. 4E).

The blood-harvested parasites were further examined for the PAD1 expression using immunofluorescence microscopy and Western blot analysis (Figs. 4 F-I). Since the PAD1 protein is specifically expressed on the surface of the BS-ST and is prominently absent from the BS-SL, it is used as a molecular marker for the former morphotype (31). At the same time, we followed characteristic morphological features, such as the distance between the kinetoplast and the nucleus and the cell volume (Figs. 4F). An exhaustive analysis failed to detect PAD1 in the HpHbR KO trypanosomes (Figs. 4H, I), which is in line with their exclusive BS-SL morphology (Figs. 4F, G). On the contrary, 97% of the WT cells were PAD1-positive (Figs. 4H, I) and had the characteristic BS-ST morphology, associated with larger cell volume and shorter distance between the kinetoplast and the nucleus (Fig. 4F). Additionally, the *in*

situ AB cells also expressed the PAD1 protein, although to a lesser extent (30%) (Figs. 4H, I), which was accompanied by the intermediate to the BS-ST phenotype (Fig. 4F).

Restoration of stumpy formation in *T. b. gambiense*

Next, we studied the consequences of a restored HpHbR expression in *T. brucei gambiense* for its life cycle progression in the mammalian host. We used the WT T. *b. gambiense* (LiTat1.3 strain; *T.b.g.* WT) and the *T. b. gambiense* cells expressing HpHbR of *T. b. brucei* from the 18S rRNA locus (*T.b.g.* +b1), as described previously (13). Both cell lines were injected into the BALB/c mice and the resulting parasitemia was followed on a daily basis. The WT parasites emerged in the bloodstream between days 2 and 3 and sustained a rather mild infection (maximum of 3 x 10^7 cells/ml was reached on day 4), as on day 6 no trypanosomes were observed in the blood smears (Fig. 5A). The *T. b. gambiense* expressing HpHbR of *T. b. brucei* triggered a yet significantly weaker infection, with cells detectable only until day 4, when they peaked at 5x10^5 cells/ml (Fig. 5A).

In the WT *T. b. gambiense*, we did not detect any PAD1-expressing cells, while the picture was strikingly different for trypanosomes, in which the *T. b. brucei* HpHbR was overexpressed. At the peak of the infection on day 4, about 25% of cells were PAD1-positive (Figs. 5B, C), associated with a significant repositioning of the nucleus towards the kinetoplast (Fig. 5D). In contrast, there was no pronounced increase in the cell volume (Fig. 5D), a feature typical for the PAD1-expressing BS-ST *T. b. brucei*.

Finally, we wondered whether the *T. b. gambiense* field isolate Bosendja (32) sustains the ability to produce waves of parasitemia. Due to its limited viability in the axenic culture, Bosendja cells were injected directly from the blood stabilates into the BALB/c mice. The parasites proliferated very rapidly in their bloodstream, reaching over 3 x 10^8 cells/ml on day 4, when the experiment was terminated (Fig. 5E). Careful morphological inspection categorized most trypanosomes into the BS-SL forms, with a pronounced undulating membrane (Fig. 5F). Although in a few cells (0.1%) expression of PAD1 was detected on day 4 by immunomicroscopy (Figs. 5F, G), The low amount of this marker protein remained undetectable by Western blot analysis, where the WT *T. b. brucei* and the *in situ* AB cells served as positive controls (Fig. 5H).

DISCUSSION

The heme group is needed for the life of almost all eukaryotic organisms analyzed so far (33). Nevertheless, it has remained unclear whether the parasitic lifestyle of trypanosomes still needs this requirement while residing in the mammalian host. Indeed, many hemoproteins are missing or downregulated in the BS *T. b. brucei*. To provide heme for its hemoproteins, such as the subunits of respiratory complexes (and enzymes involved in the sterol synthesis (17), the BS and PS *T. b. brucei* scavenge heme from their hosts *via* the HpHbR and *Tb*Hrg receptors, respectively (6, 9).

The HpHbR of *T. brucei s.l.* has undergone a remarkable set of adaptations, likely triggered by coevolution with their distinct hosts. To avoid lysis by the innate immunity factors in the blood of primates, the HpHbR of *T. b. gambiense* acquired specific mutations that decreased the affinity towards its ligand (10, 11, 13). Its lower affinity for TLF as compared to HpHb led to the proposal that the cells maintain the HpHb uptake while resisting lysis (12). The closely related *T. congolense* and *T. vivax* use HpHbR to take up Hb rather than HpHb from the digested blood (34). Moreover, while in *T. brucei s. l.* HpHbR is confined to the flagellar pocket, where it was shown to be down-regulated during the stumpy formation (27), it is present on the cell surface of the *T. congolense* epimastigotes (35) at a density ~1000-fold higher than in the BS *T. b. brucei* (34).

Following confirmation of the lack of heme *b* detected in the BS *T. b. brucei* devoid of HpHbR (6), here we have shown that WT BS *T. b. gambiense* also contains minimal if any heme. We imply that the BS trypanosomes can grow in limited amounts of heme, suggesting a lack of essentiality of this ancient cofactor in this life cycle stage. As we reported earlier, heme is also dispensable for the plant trypanosomatid parasite *Phytomonas serpens.* Cells that were grown without heme incorporated lanosterol into the membranes instead of ergosterol, overcoming the need for hemoprotein CYP51 (36). In this study, we focused on the hemoprotein CYP51 in *T.brucei,* where we have shown that CYP51 is not essential for BS parasites and represents an acceptor of the HpHbR-imported heme. We have further evaluated the HpHbR-dependent CYP51 inhibition in the WT *T. b. rhodesiense* by modulating its access to the cognate ligand of the receptor and proved a positive correlation between an operational HpHb uptake and the cytokinetic CYP51 activity.

Moreover, to have a readout for potent heme-dependent activity, we have overexpressed human catalase (37) in the WT and HpHbR KO *T. b. brucei*, as well as in the

WT *T. b. gambiense*. The data conclusively showed that in *T. b. brucei* BS HpHbR internalizes heme, which is subsequently incorporated into the cytosolic hemoprotein.

Under physiological conditions, human blood is low in free Hb. Lysed erythrocytes release an excess of Hb that binds to Hp with a picomolar affinity and forms a complex internalized by macrophages (38). Trypanosomes imitate this process *via* their HpHbR, which competes for the ligand (39). Impaired erythrocytes and their clearance eventually cause anemia, which represents the primary pathological hallmark of animal trypanosomiasis (40). Intriguingly, reports of severe infection-associated anemia are missing for human *T. b. gambiense* infections, which can be even asymptomatic (41).

The erythrocytes from mice infected with trypanosomes exhibit an enhanced osmotic fragility and altered fatty acid membrane composition (42), which are caused by both host immune response and parasite-derived factors (43). It was also proposed that during the acute phase of mice infection, *T. b. brucei* releases extracellular vesicles that fuse with erythrocytes and consequently increase their fragility and clearance (44). We propose that trypanosome infection related Hb-release may be one of the factors modulating the course of parasitic waves and deserves a closer look.

One of the main processes which are associated with parasitemia control in the mammalian host is the transition from the dividing BS-SL to the quiescent BS-ST (45). Recently, several proteins and effector molecules involved in this complex process have been described (30, 46, 47). The fact that in the absence of HpHbR, the key BS-SL to BS-ST transition is disrupted, prompts us to suggest that heme uptake may be an additional player in this life cycle progression. This assumption is further backed by our observation that the WT *T. b. gambiense* has a poor capability to generate typical BS-ST. Importantly, a mere replacement of the *T. b. gambiense* HpHbR by its functional *T. b. brucei* variant restores the capacity to progress into this life cycle stage. The accelerated pathogenicity for mice of *T. b. brucei* devoid of HpHbR is likely caused by the fast division of the BS-SL and the failure to develop into the non-dividing BS-ST, which would otherwise lead to protracted progress of the infection.

HpHbR is known to be a gateway for the internalization of TLF, which results in the lysis of *T. b. brucei* by human serum (39). Here we show that in *T. b. gambiense,* this receptor also effectively prevents the import of heme with consequences for the heme-requiring cellular processes. While this would be lethal for a typical aerobic eukaryote that depends on

external heme, trypanosomatids, such as the abovementioned *Phytomonas* have a unique capacity to tolerate complete heme deficiency (36).

Changes in *T. b. gambiense* HpHbR seems to have far-reaching consequences with decreased and eventually abrogated heme import. Heme dispensability may be associated with lower pathogenicity and possibly result in the chronic form of the disease. However, unless experimentally tested, this will remain speculation backed by the lower pathogenicity of the HpHbR KO *T. b. brucei* for both the Hp-carrying and Hp-lacking mice (6).

Importantly, trypanosomes with defective HpHbR (*T.b.b*. HpHbR KO; *T.b.g*. WT) are struggling to progress into the BS-ST, which was so far considered the only stage of *T. brucei s.l.* capable of transmission to tsetse flies (47). However, this postulation has been challenged very recently (48), showing that *T.b.b*. BS-SL and BS-ST trypanosomes are equally capable of infecting tsetse flies. The transmissibility via tsetse fly of *T. b. gambiense* is known to be poor even under controlled experimental conditions, for so far unknown reasons (49, 50, J. V. d. A., unpubl. data). To the best of our knowledge, the reporting of putative BS-ST cells in *T. b. gambiense* was based solely on morphological criteria (51, 52) and may have resulted in a misassignment to a different *T. brucei* sub-species that is more prone to BS-ST transition. More recent publications describe a high variability in the proportion of the BS-SL to BS-ST cells in different field strains of *T. b. gambiense* (50, 53). Moreover, no clear correlation was noted between the presence of the putative BS-ST and transmissibility via tsetse flies (53), further questioning the relevance of the BS-ST cells in *T. b. gambiense*.

In summary, we submit that the consequence of the unique metabolic independence on heme described above for *T. b. gambiense*, which accounts for a vast majority of human infections, resulted in the loss of transmission-competent PAD1-expressing BS-ST cells from their life cycle. This disadvantage may be compensated by lower pathogenicity and significantly prolonged chronic disease typical for *T. b. gambiense*-caused human African sleeping sickness.

EXPERIMENTAL PROCEDURES

Cells growth and differentiation

Bloodstream *T. b. brucei* 90-13 (328-114 single marker), *T. b. rhodesiense* EtTat1.2R and *T. b. gambiense* AnTat 1.3 were routinely cultivated at 37 °C in HMI-9 medium (Thermo Fisher), supplemented with 20% heat-inactivated foetal bovine serum. Bloodstream *T. b. brucei* 427

was grown in the same medium with 10% fetal bovine serum. Field isolate of *T. b. gambiense* (Bosendja; AnTAR 6; ZR/ KIN001) was kept by passaging in mice. Cell densities were measured using the Z2 Coulter counter (Beckman Coulter) or by hemocytometer.

Transgenic cell lines

Procyclic *T. b. brucei* 29-13 CYP51 RNAi and HpHbR-KO (328-114) cell lines were described previously (6, 54). *T. b. brucei* CYP51-KO (328-114) and 90-13 HpHbR-KO cell lines were generated by successive deletion of alleles with pPuro-KO or pHygro-KO, and pPhleo-KO constructs (13). The pTSArib HpHbR construct used to complement the 90-13 HpHbR-KO cell line was obtained by subcloning of HpHbR ORF into pTSARib Ble (blasticidin resistance) plasmid (23). The other constructs designed to modulate the level of HpHbR expression were generated from the pET-*in situ* construct (55) after the replacement of the hygromycin resistance gene by Ble. PCR-amplified DNA fragments were assembled and cloned into pET-*in situ* Ble plasmid by recombination (InFusion, Clontech). The constructs are depicted in Suppl. Fig. 2. Trypanosomes were transfected with linearized plasmid DNA or with gel-purified PCR products as described elsewhere (56). Selection markers were applied 6 hours post-transfection, and clones were generated by limited dilution.

Real-time PCR, Western blot analysis and Luciferase activity measurement

Total RNA was extracted using Trizol reagent, and the cDNA was synthesized using the PrimeScript™ RT Reagent Kit with gDNA Eraser (Takara) as described by the manufacturer with an oligo dT used instead of random primers. The qRT-PCR was performed with the cDNA using the SYBR-green stain (Takara). Primers used for HpHbR gene were FW 5'CCAATGTCGAGGTCGCCATGGCTGAGGGTTTAAAAACCAAAGACGAAG 3' and RV 5'CCAATGTGCGGCCGCAAGCTTGGCATAACTGCGGAAACCACTAACCAC 3'. The C1 primers (FW 5'TTGTGACGACGAGAGCAAAC 3' and RV 5'GAAGTGGTTGAACGCCAAAT 3') were used as endogenous control (57).

In order to detect protein expression in the bloodstream stage, lysates from $5x10^6$ cells were separated on a 12% SDS-polyacrylamide gel, transferred to a PVDF membrane and probed with the monoclonal anti-V5 and anti-α tubulin antibodies (Thermo Fisher) at 1:2,000 and 1:5,000 dilutions, respectively. Alternatively, the samples were prepared the same way

(except the lysates were not boiled but heated to 37 °C) and probed with anti-PAD1 and anti-enolase antibodies at 1:1,000 and 1: 10,000 dilutions, respectively.

2×10^6 parasites were centrifuged, lysed and labeled by the Luciferase Assay kit as recommended by the manufacturer (Promega). The readout was performed for 10 seconds with Luminoskan TL Plus instrument (Labsystems).

Overexpression and activity assay for catalase

The construct for expression of human catalase (hCAT, NCBI gene ID NP_001743.1) was modified from the one described previously (37) to be constitutively expressed. The obtained constructs were linearized by *Not*I, electroporated into the bloodstreams of *T. b. brucei* and *T.b.gambiense* and selected using 1 μg/ml hygromycin (Thermo Fisher).

The activity of catalase was monitored by respirometry using Oxygraph-2K (Oroboros) as an amount of O_2 produced after the addition of H_2O_2 and analyzed using the Oroboros DatLab Software. *T. b. brucei* 90-13 *and T. b. gambiense* LiTat 1.3 WT were used to establish the background of the respirometry experiment. Briefly, 1×10^6 of bloodstream cells resuspended in 2 ml of HMI-9 medium were treated with 20 μl of 882 mM (3%) H_2O_2. Alternatively, 5×10^6 parasites were resuspended in 10 μl phosphate buffered saline (PBS) and placed on a microscopic slide. The same volume of 3% H_2O_2 was added to the cells, mixed, and the formation of oxygen visible as macroscopic bubbles was monitored as a readout for the catalase activity. All measurements and statistics were calculated from three independent biological replicates.

Indirect immunofluorescence assay

For immunofluorescence analysis, 1×10^6 to 1×10^7 cells were fixed with 4% paraformaldehyde and settled on microscopic slides. After 10 min incubation at room temperature, they were washed with PBS and permeabilized with 100% ice-cold methanol for 20 min. Cells were incubated with 5% fat-free milk in PBS-Tween (0.05%) for 1 h, followed by incubation with primary anti-V5, anti-PAD1 or anti-CYP51 at 1:1,000 dilutions and secondary Alexa Fluor-488 or Alexa Fluor-555 anti-rabbit IgG antibodies (Thermo Fisher) at 1:1,000 dilution for 1 hr at room temperature. After the last washing step, cells were stained with DAPI, mounted with an anti-fade reagent (Thermo Fisher) and visualized using a fluorescent microscope Zeiss Axioplan 2 (Carl Zeiss).

High-performance liquid chromatography

A total of $5x10^8$ bloodstream cells was harvested by centrifugation at 1,000 g at 4°C for 10 min and washed 3 times with PBS on ice. Cells were resuspended in 60 µl H_2O, extracted with 400 µl acetone/0.2% HCl, and the supernatant was collected after centrifugation at 1,000 g at 4°C for 5 min. The pellet was resuspended in 200 µl acetone/0.2% HCl and centrifuged as described above. Both supernatants were combined, and 150 µl of each sample was immediately injected into a high-performance liquid chromatography system (Infinity 1200, Agilent Technologies) and separated using a reverse-phase column (4 µm particle size, 3.9 x 75 mm) (Waters) with 0.1 % trifluoroacetic acid and acetonitrile/0.1% trifluoroacetic acid as solvents A and B, respectively. Heme *b* was eluted with a linear gradient of solvent B (30–100% in 12 min) followed by 100% of B at a flow rate of 0.8 ml/min at 40°C. Heme was detected by diode array detector (Infinity 1200, Agilent Technologies) and identified by retention time and absorbance spectra according to commercially available standard (Sigma-Aldrich).

Fly and mouse infections

Teneral tsetse flies were fed, 24–48 hours after emergence, with *T. b. brucei* Antat 1.1 WT and HpHbR-3'PAD1 strains infected blood meal, either or not supplemented with 10 mM reduced L-glutathione to increase infection establishment. Parasites were harvested from the blood of cyclophosphamide-immunosuppressed mice (Endoxan) at 6–7 days post-infection and mixed with defibrinated horse blood (E&O Laboratories). Flies were further fed every 2–3 days on uninfected defibrinated horse blood. Then, flies were dissected on day 10 after the first blood meal to assess the presence of parasites in the midgut (i.e. establishment of a PS midgut infection)

Four to six-week-old BALB/c mice were intraperitoneally injected with 1×10^4 (*T.b. brucei* strains) or $3x10^6$ (*T.b. gambiense* strains) bloodstream cells. The infection was followed daily by diluting tail snip blood in TrypFix buffer (3.7% formaldehyde, 1×SSC buffer) and manual counting of trypanosomes in a Neubauer hemocytometer. Mice were euthanized for the collection of parasites, which were separated from the erythrocytes on a diethylaminoethyl (DEAE) cellulose column using a standard protocol. Purified trypanosomes were washed once with PBS and subsequently used for downstream experiments.

Hp-488 preparation and labeling

Hp was conjugated with Alexa 488 using the Dylight amine-reactive kit (Thermo Fischer) as recommended by the manufacturer. The blood from mice was collected at different times of infection from a tail puncture with a capillary containing heparin and centrifuged at 12,000 rpm for 3 min to separate the parasites, which were subsequently incubated at 37^{o}C for 15 min in HMI-9 medium containing the lysosomal protease inhibitor FMK-024. The parasites were incubated in 20 µg/ml (f. c.) Alexa 488-labeled Hp for 2 hrs, subsequently fixed with 4% paraformaldehyde for 10 min, stained with DAPI and analyzed with a Zeiss Axioplan 2 epifluorescence microscope equipped with a Zeiss AxioCam HRm digital camera (Carl Zeiss, Thornwood, NY). Resulting images were analyzed using Adobe Photoshop software and Fiji.

Ethics statement

In Czech Republic, the research was approved by the Central Commission for Animal Welfare, Biology Centre (protocol No. 28/2016). All experimental procedures complied with the Czech law (Act No. 246/1992). In Belgium, the research was approved by the animal ethics committee of the Institute for Molecular Biology and Medicine and the Institute of Tropical Medicine (tsetse fly infection experiment). All mice were housed in a pathogen-free facility and the experiments were performed in compliance with the relevant laws and institutional guidelines (license LA1500474).

REFERENCES

1. Franco, J.R., Simarro, P.P., Diarra, A. & Jannin, J.G. Epidemiology of human African trypanosomiasis. *Clin. Epidemiol*. **6**, 257-75 (2014).

2. Hajduk, S.L. et al. Lysis of *Trypanosoma brucei* by a toxic subspecies of human high-density lipoprotein. *J. Biol. Chem*. **264**, 5210-5217 (1989).

3. Raper, J., Portela, M.P., Lugli, E., Frevert, U. & Tomlinson, S. Trypanosome lytic factors: novel mediators of human innate immunity. *Curr. Opin. Microbiol.* **4**, 402–408 (2001).

4. Smith, A.B., Esko, J.D. & Hajduk, S.L. Killing of trypanosomes by the human haptoglobin-related protein. *Science* **268**, 284-286 (1995).

5. Vanhamme, L. et al. Apolipoprotein L-I is the trypanosome lytic factor of human serum. *Nature* **422,** 83–87 (2003).

6. Vanhollebeke, B. et al. A haptoglobin-hemoglobin receptor conveys innate immunity to *Trypanosoma brucei* in humans. *Science* **320**, 677-681 (2008).

7. Stødkilde, K., Torvund-Jensen, M., Moestrup, S.K. & Andersen, C.B. Structural basis for trypanosomal haem acquisition and susceptibility to the host innate immune system. *Nat. Commun*. **5**, 5487 (2014).

8. Kořený, L., Lukeš, J., & Oborník, M. Evolution of the haem synthetic pathway in kinetoplastid flagellates: an essential pathway that is not essential after all? *Int. J. Parasitol.* **40**, 149–156 (2010).

9. Horáková, E. et al. The *Trypanosoma brucei* TbHrg protein is a heme transporter involved in regulation of stage-specific morphological transitions*. J. Biol. Chem.* **292**, 6998-7010 (2017).

10. DeJesus, E., Kieft, R., Albright, B., Stephens, N.A. & Hajduk, S.L. Single amino acid substitution in the group 1 *Trypanosoma brucei gambiense* haptoglobin-hemoglobin receptor abolishes TLF-1 binding. *PLoS Pathog*. **9**, e1003317 (2013).

11. Symula, R.E. et al. *Trypanosoma brucei gambiense* group 1 is distinguished by a unique amino acid substitution in the HpHb receptor implicated in human serum resistance. *PLoS Negl. Trop. Dis*. **6**, e1728 (2012).

12. Higgins, M.K. et al. Structure of the trypanosome haptoglobin hemoglobin receptor and implications for nutrient uptake and innate immunity. *Proc. Natl Acad. Sci. USA* **110**, 1905–1910 (2013).

13. Uzureau, P. et al. Mechanism of *Trypanosoma brucei gambiense* resistance to human serum. *Nature* **501**, 430-434 (2013).

14. Higgins, M.K., Lane-Serff, H., MacGregor, P. & Carrington M. A. Receptor's tale: An eon in the life of a trypanosome receptor. *PLoS Pathog*. **26**, 13:e1006055 (2017).

15. Kraeva, N. et al. Catalase in Leishmaniinae: With me or against me? *Infect. Genet. Evol*. **50**, 121-127 (2017).

16. Zhou, W., Cross, G.A. & Nes, W.D. Cholesterol import fails to prevent catalyst-based inhibition of ergosterol synthesis and cell proliferation of *Trypanosoma brucei*. *J. Lipid. Res*. **48**, 665-673 (2007).

17. Nes, C.R. et al. Novel sterol metabolic network of *Trypanosoma brucei* procyclic and bloodstream forms. *Biochem. J*. **443**, 267-277 (2012).

18. Kessler, R.L., Soares, M.J., Probst, C.M. & Krieger M.A. *Trypanosoma cruzi* response to sterol biosynthesis inhibitors: morphophysiological alterations leading to cell death. *PLoS ONE* **8**, e55497 (2013).

19. McCall, L.I. et al. Targeting ergosterol biosynthesis in *Leishmania donovani*: essentiality of sterol 14alpha-demethylase. *PLoS Negl. Trop. Dis*. **9**, e0003588 (2015).

20. Dauchy, F.A. et al. *Trypanosoma brucei* CYP51: essentiality and targeting therapy in an experimental model. *PLoS Negl. Trop. Dis*. **10**, e0005125 (2016).

21. Zhang, J. et al. The Fungal CYP51s: Their functions, structures, related drug resistance and inhibitors. *Front. Microbiol*. **10**, 691 (2019).

22. Lepesheva, G.I. et al. Sterol 14alpha-demethylase as a potential target for antitrypanosomal therapy: enzyme inhibition and parasite cell growth. *Chem. Biol.* **14**, 1283-1293 (2007).

23. Lecordier. L. et al. Adaptation of *Trypanosoma rhodesiense* to hypohaptoglobinaemic serum requires transcription of the APOL1 resistance gene in a RNA polymerase I locus. *Mol. Microbiol.* **97**, 397-407 (2015).

24. Koda, Y., Soejima, M., Yoshioka, N. & Kimura, H. The haptoglobin-gene deletion responsible for anhaptoglobinemia. *Am J Hum Genet*. **62**, 245-252 (1998).

25. Vanhollebeke, B. et al. Distinct roles of haptoglobin-related protein and apolipoprotein L-I in trypanolysis by human serum. *Proc. Natl. Acad. Sci. USA* **104**, 4118-4123 (2007).

26. Clayton, C. Regulation of gene expression in trypanosomatids: living with polycistronic transcription. *Open Biol*. **9**, 190072 (2019).

27. Vanhollebeke, B., Uzureau, P., Monteyne, D., Pérez-Morga, D. & Pays, E. Cellular and molecular remodeling of the endocytic pathway during differentiation of *Trypanosoma brucei* bloodstream forms. *Eukaryot. Cell* **9**,1272–1282 (2010).

28. MacGregor, P. & Matthews, K.R. Identification of the regulatory elements controlling the transmission stage-specific gene expression of PAD1 in Trypanosoma brucei. *Nucleic Acids Res*. **40(16)**, 7705-7717 (2012).

29. MacLeod, E.T., Maudlin, I., Darby, A.C. & Welburn, S.C. Antioxidants promote establishment of trypanosome infections in tsetse. *Parasitology* **134**, 827-831 (2007).

30. Rojas, F. et al. Oligopeptide signaling through TbGPR89 drives trypanosome quorum sensing. *Cell* **176**, 306-317 (2019).

31. Silvester, E., McWilliam, K.R. & Matthews, K.R. The cytological events and molecular control of life cycle development of *Trypanosoma brucei* in the mammalian bloodstream. *Pathogens* **6**, 29 (2017).

32. Fontaine, F. et al. APOLs with low pH dependence can kill all African trypanosomes. *Nat. Microbiol*. **2**, 1500–1506 (2017).

33. Hamza, I. & Dailey, H.A. One ring to rule them all: Trafficking of heme and heme synthesis intermediates in the metazoans. *Biochim. Biophys. Acta* **1823**, 1617-1632 (2012).

34. Lane-Serff, H. et al. Evolutionary diversification of the trypanosome haptoglobin-haemoglobin receptor from an ancestral haemoglobin receptor. *eLife* **5**, e13044 (2016).

35. Eyford, B.A. et al. Differential protein expression throughout the life cycle of *Trypanosoma congolense*, a major parasite of cattle in Africa. *Mol. Biochem. Parasitol*. **177**, 116–125 (2011).

36. Kořený, L. et al. Aerobic kinetoplastid flagellate Phytomonas does not require heme for viability. *Proc. Natl. Acad. Sci. USA* **109**, 3808–3813 (2012).

37. Horáková, E. et al. Catalase compromises the development of the insect and mammalian stages of *Trypanosoma brucei*. *FEBS J*. **287**, 964-977 (2020).

38. Kristiansen, M. et al. Identification of the hemoglobin scavenger receptor. *Nature* **409**, 198–201 (2001).

39. Vanhollebeke, B. & Pays, E. The trypanolytic factor of human serum: many ways to enter the parasite, a single way to kill. *Mol. Microbiol*. **76**, 806-814 (2010).

40. Radwanska, M., Vereecke, N., Deleeuw, V., Pinto, J. & Magez, S. Salivarian trypanosomosis: A review of parasites involved, their global distribution and their interaction with the innate and adaptive mammalian host immune system. *Front. Immunol.,* **9**, 2253 (2018).

41. Büscher, P. et al. Do cryptic reservoirs threaten gambiense-sleeping sickness elimination? *Trends Parasitol*. **34**, 197-207 (2018).

42. Cnops, J. et al. NK-, NKT- and CD8-derived IFNγ drives myeloid cell activation and erythrophagocytosis, resulting in trypanosomosis-associated acute anemia. *PLoS Pathog*. **11**, e1004964 (2015).

43. Stijlemans, B., de Baetselier, P., Magez, S., van Ginderachter, J.A. & De Trez, C. African trypanosomiasis-associated anemia: the contribution of the interplay between parasites and the mononuclear phagocyte system. *Front Immunol*. **9**, 218 (2018).

44. Szempruch, A.J. et al. Extracellular vesicles from *Trypanosoma brucei* mediate virulence factor transfer and cause host anemia. *Cell* **164**, 246–257 (2016).

45. Seed, J.R. & Wenck, M.A. Role of the long slender to short stumpy transition in the life cycle of the African trypanosomes. *Kinetopl. Biol. Dis*. **2**, 3 (2003).

46. Mony, B.M. et al. Genome-wide dissection of the quorum sensing signalling pathway in *Trypanosoma brucei*. *Nature* **505**, 681–5 (2014).

47. Rojas, F. & Matthews, K.R. Quorum sensing in African trypanosomes. *Curr. Opin. Microbiol.* **52**, 124-129 (2019).

48. Schuster, S. et al. A modification to the life cycle of the parasite *Trypanosoma brucei.* bioRxiv717975; doi: https://doi.org/10.1101/717975 (2019).

49. Le Ray, D. Vector susceptibility to African trypanosomes. *Ann. Soc. Belg. Med. Trop*. **69**, 165-214 (1989).

50. Ravel, S., Patrel, D., Koffi, M., Jamonneau, V. & Cuny, G. Cyclical transmission of *Trypanosoma brucei gambiense* in *Glossina palpalis gambiensis* displays great differences among field isolates. *Acta Trop*. **100**, 151-155.

51. Wijers, D.J., & Willett, K.C. (1960). Factors that may influence the infection rate of *Glossina palpalis* with *Trypanosoma gambiense*. II. The number and morphology of the trypanosomes present in the blood of the host at the time of the infected feed. *Ann. Trop. Med. Parasitol*. **54**, 341-350 (2006).

52. Brickman, M.J. & Balber, A.E. *Trypanosoma brucei brucei* and *T. b. gambiense*: stumpy bloodstream forms express more CB1 epitope in endosomes and lysosomes than slender forms. *J Eukaryot. Microbiol*. **41**, 533-536 (1994).

53. Janelle, J. et al. Monitoring the pleomorphism of *Trypanosoma brucei gambiense* isolates in mouse: impact on its transmissibility to *Glossina palpalis gambiensis*. *Infect. Genet. Evol*. **9**, 1260-1264 (2009).

54. Haubrich, B.A. et al. Discovery of an ergosterol-signaling factor that regulates *Trypanosoma brucei* growth. *J. Lip. Res*. **56**, 331-341 (2015).

55. Kelly, S. et al. Functional genomics in Trypanosoma brucei: a collection of vectors for the expression of tagged proteins from endogenous and ectopic gene loci. *Mol Biochem Parasitol*. **154(1)**,103-109 (2007).

56. Burkard, G., Fragoso, C.M. & Roditi, I. Highly efficient stable transformation of bloodstream forms of *Trypanosoma brucei*. *Mol. Biochem. Parasitol*. **153**, 220–223 (2007).

57. Jones, N.G. et al. Regulators of *Trypanosoma brucei* cell cycle progression and differentiation identified using a kinome-wide RNAi screen. *PLoS Pathog.* **10**, e1003886 (2014).

ACKNOWLEDGEMENTS

We thank Eva Kriegová and Zuzana Vavrušková (Institute of Parasitology) for help with animal experiments. We thank Nick Van Reet (Institute of Tropical Medicine, Antwerp) for providing the field strains of *T.b. gambiense*. This work was supported by the ERC CZ project LL1601 to J.L., ERD Funds project OPVVV 0000759, and Czech Grant Agency projects 18-15962S and 20-07186S.

AUTHOR CONTRIBUTIONS

Conceptualization, B.V., E.H.; Methodology, E.H., L.L., R.S., B.V.; Investigation, E.H., L.L., P.Cunha., R.S., P. Changmai., C.J.M.L., J.V.D.A., B.V.; Resources, B.V. and J.L.; Writing, E.H., L.L., P.Cunha, J.V.D.A., B.V. and J.L.

DECLARATION OF INTERESTS

The authors declare no competing interests.

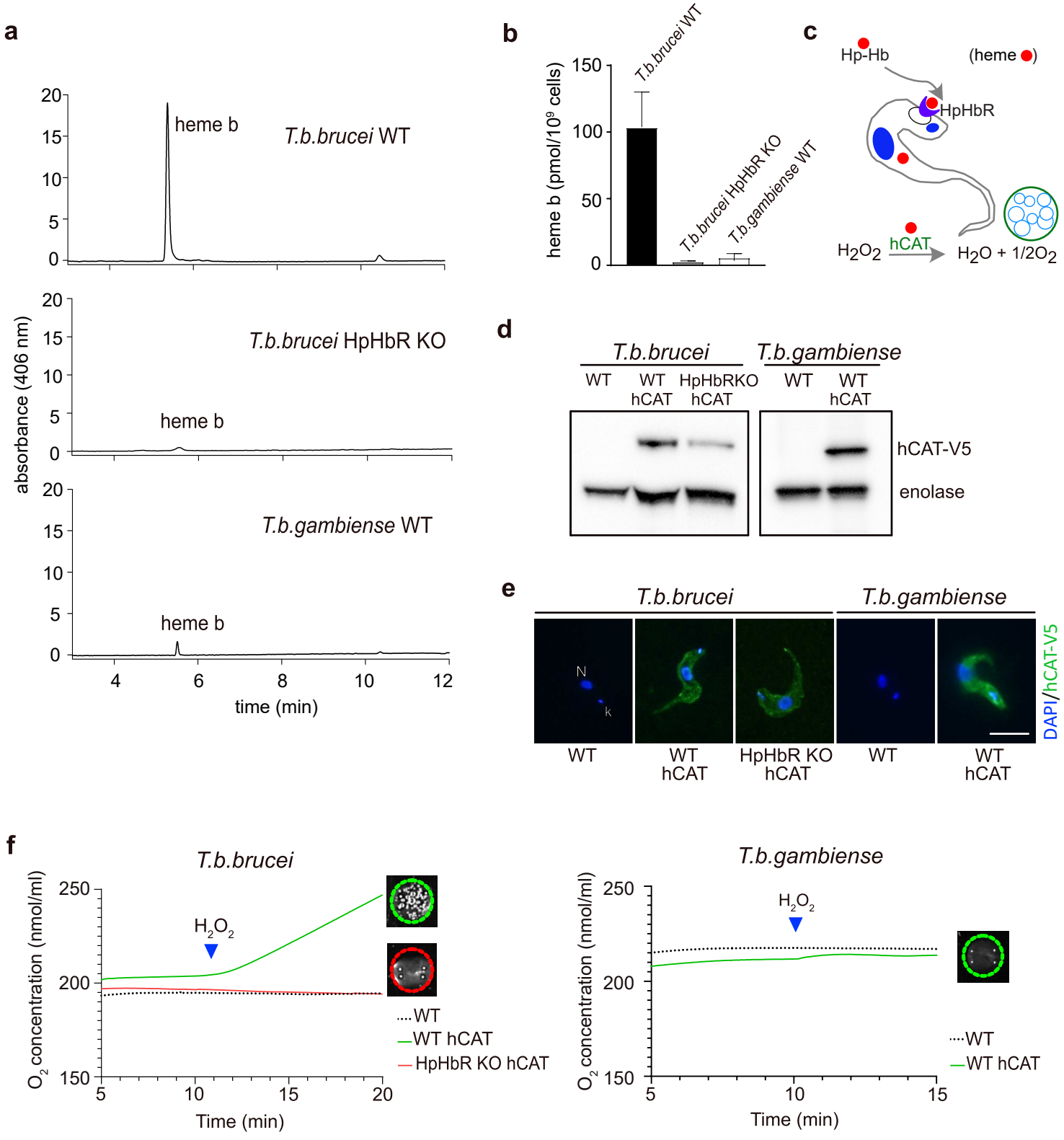

Figure 1. Detection of heme and hemoproteins in bloodstream stages of *T. b. brucei* and *T. b. gambiense*
(**a**) Heme *b* extracted from 1 x 10^9 cells was separated by HPLC and detected by a diode array detector. Representative chromatogram from wild type *T. b. brucei*, *T. b. brucei* knock-out for HpHbR and wild type *T. b. gambiense*. (**b**) Graph showing quantification of total heme *b* content in the same cell lines as in (a); (n = 3). (**c**) Schematic representation of the experimental design used for the measurement of the activity of the N-terminally V5-tagged human catalase (hCAT) in bloodstream *T. brucei*. (**d**) Western blot analysis with V5 antibody that detects human catalase (hCAT) in WT and HpHbR knock-out (KO) of *T. b. brucei* and WT *T. b. gambiense* overexpressing hCAT. Enolase was used as a loading control. (**e**) Immunofluorescence of hCAT detected with V5 antibody (green) in the same cell lines as in (d). DNA in the nucleus (N) and kinetoplast (k) was stained with DAPI (blue). Scale bar, 5 μm. (**f**) Measurement of the activity of human catalase using Oroboros oxygraph in *T. b. brucei* (left) and *T. b. gambiense* (right); (n=3). Visual verification of measured activity *via* the O_2 production in the form of bubbles after the addition of 3% H_2O_2 is shown in insets.

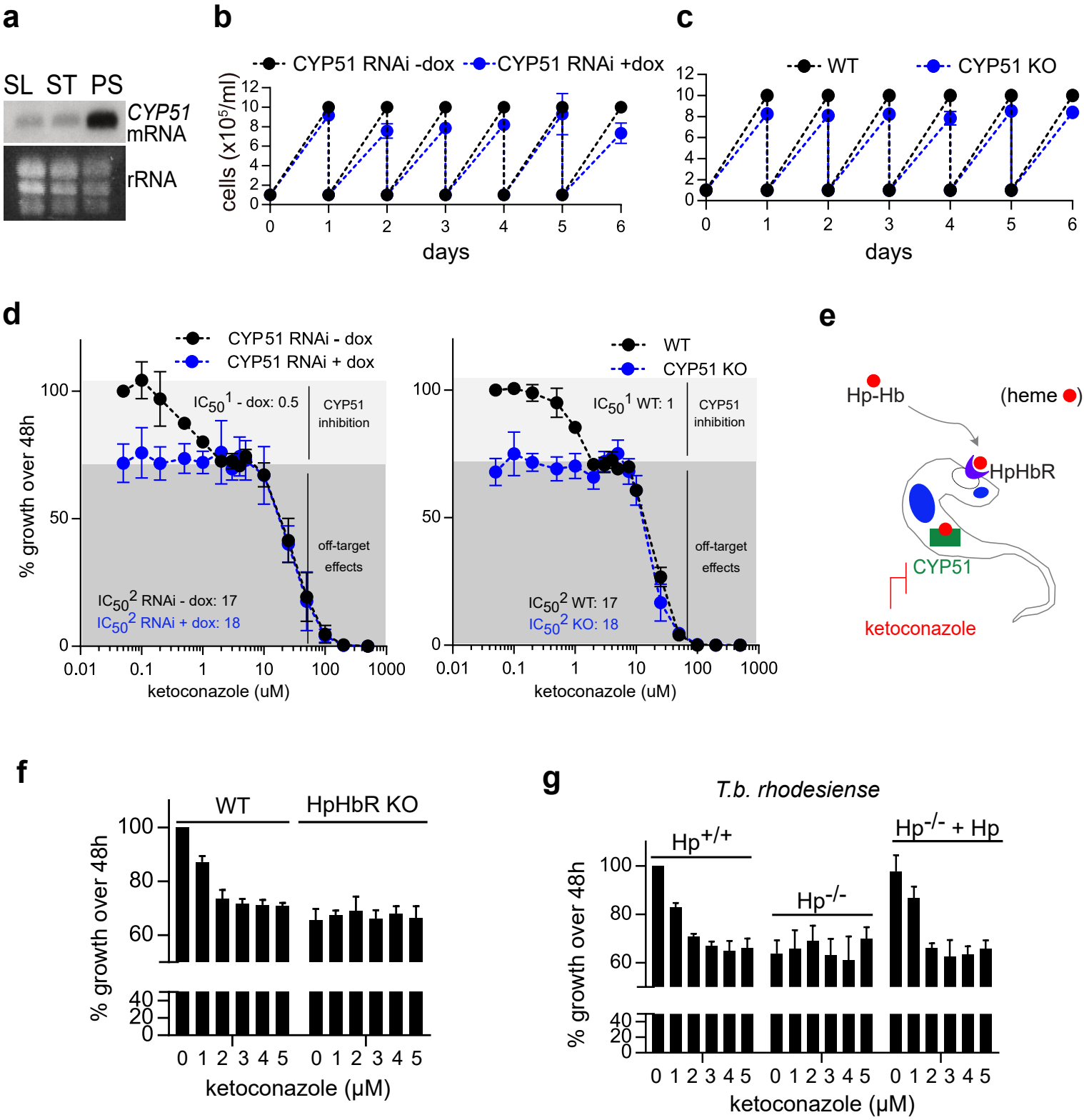
a
SL ST PS
CYP51 mRNA
rRNA
b
CYP51 RNAi -dox
CYP51 RNAi +dox
cells (x10^5/ml)
days
c
WT
CYP51 KO
days
d
CYP51 RNAi - dox
CYP51 RNAi + dox
IC50^1 - dox: 0.5
CYP51 inhibition
off-target effects
IC50^2 RNAi - dox: 17
IC50^2 RNAi + dox: 18
% growth over 48h
ketoconazole (uM)
WT
CYP51 KO
IC50^1 WT: 1
CYP51 inhibition
off-target effects
IC50^2 WT: 17
IC50^2 KO: 18
ketoconazole (uM)
e
Hp-Hb
(heme)
HpHbR
CYP51
ketoconazole
f
WT
HpHbR KO
% growth over 48h
ketoconazole (μM)
g
T.b. rhodesiense
Hp+/+
Hp-/-
Hp-/- + Hp
% growth over 48h
ketoconazole (μM)

Figure 2. Effect on growth and ketoconazole sensitivity after CYP51 invalidation in the bloodstream stage

(**a**) Northern blot analysis showing stage-specific expression of *CYP51* mRNA. Total RNA from long slender (SL) and stumpy (ST) bloodstream stage, and procyclic stage (PS) was hybridized with the *Tb*CYP51 DNA probe. The staining of ribosomal (r)RNA was used as a loading control. (**b**) Growth curves of *T. b. brucei* bloodstreams in the presence (blue dots and line) and absence (black dots and line) of doxycycline (dox), which induces CYP51 RNAi for 6 days. (**c**) Growth curves of WT *T. b. brucei* (black dots and line) and CYP51 knock-out (KO) (blue dots and line) for 6 days. (**d**) The depletion of CYP51 confers insensitivity to low doses of ketoconazole. Left: CYP51 RNAi cells were grown with doxycycline to induce RNAi (blue dots and line) or without it (non-induced cells; black dots and line), during 48 h exposure to ketoconazole. Right: WT (black dots and line) and CYP51 knock-out (KO) cells (blue dots and line) were grown under the same conditions. A grey zone indicates concentrations of ketoconazole without inhibitory effect on CYP51. (**e**) Schematic representation of the experimental design showing the inhibition of hemoprotein CYP51 activity by ketoconazole. (**f**) Deficiency in the haptoglobin-hemoglobin (HpHb) uptake results in mild growth phenotype and insensitivity to the CYP51 inhibitor. WT *T. b. brucei* and HpHbR knock-out (KO) were incubated for 48 h with 0 to 5 μM of ketoconazole. (**g**) *T. b. rhodesiense* Etat 1.2R cells freshly isolated from mice and transferred to *in vitro* culture conditions with either normal human serum containing HpHb (Hp+/+), human serum lacking Hp (anhaptoglobinemic) (Hp-/-), or anhaptoglobinemic serum complemented with purified human Hp (Hp-/- + Hp). Their growth rate was determined after incubation for 48 h with 0 to 5 μM of ketoconazole.

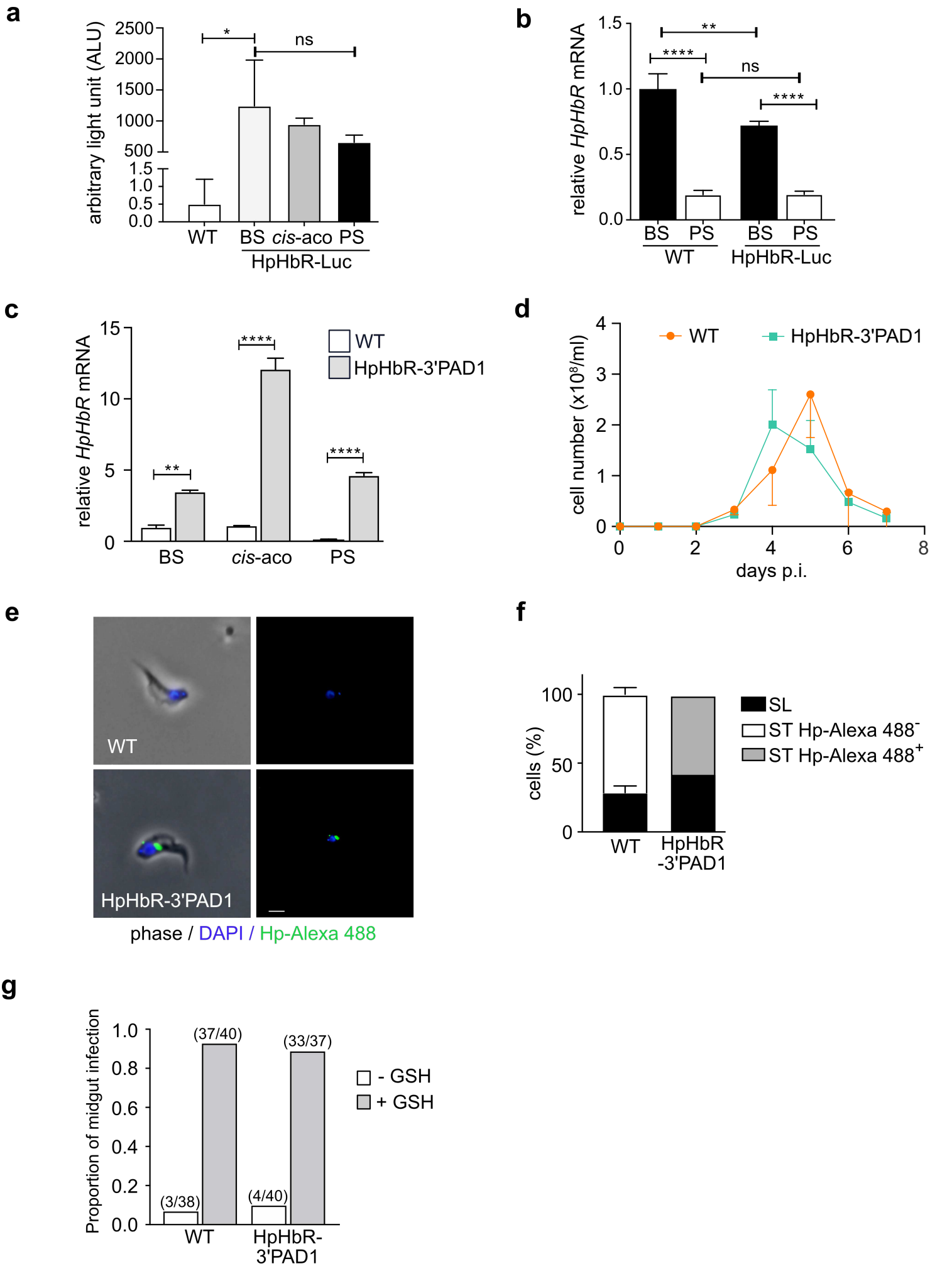
a
arbitrary light unit (ALU)
2500
2000
1500
1000
500
1.5
1.0
0.5
0.0
*
ns
WT
BS
cis-aco
PS
HpHbR-Luc
b
relative HpHbR mRNA
1.5
1.0
0.5
0.0
**
****
ns
****
BS
PS
BS
PS
WT
HpHbR-Luc
c
relative HpHbR mRNA
15
10
5
0
**
****
****
WT
HpHbR-3'PAD1
BS
cis-aco
PS
d
cell number (x10⁸/ml)
4
3
2
1
0
WT
HpHbR-3'PAD1
0
2
4
6
8
days p.i.
e
WT
HpHbR-3'PAD1
phase / DAPI / Hp-Alexa 488
f
cells (%)
100
50
0
SL
ST Hp-Alexa 488⁻
ST Hp-Alexa 488⁺
WT
HpHbR
-3'PAD1
g
Proportion of midgut infection
1.0
0.8
0.6
0.4
0.2
0.0
(37/40)
(33/37)
(3/38)
(4/40)
- GSH
+ GSH
WT
HpHbR-
3'PAD1

Figure 3. Artificial expression of HpHbR in stumpy form does not interfere with life cycle progression

(**a**) *T. b. brucei* engineered to express *Luciferase* along with *HpHbR* at the end of the polycistronic transcription unit (HpHbR-Luc). Luciferase activity was measured during *in vitro* differentiation in the bloodstream stage (BS), 2 h after differentiation was triggered by *cis*-aconitate (*cis*-aco), and the procyclic stage (PS), as well as in wild types (WT) used as a control. (**b**) RT-PCR assessed the expression of HpHbR in WT and HpHbR-Luc cells. Complementary DNA was synthesized from RNA extracted from the bloodstream (BS) and procyclic stages (PS) and used for RT-PCR as described in experimental procedures. (**c**) The expression of HpHbR was assessed as in (b) in the WT *T. b. brucei* and HpHbR-3'PAD1 trypanosomes. RNA was extracted from the BS, 2 h after differentiation was triggered by *cis*-aconitate (*cis*-aco) and the procyclic stage (PS). (**d**) *In vivo* infectivity of WT *T. b. brucei* and HpHbR-3'PAD1 cells was evaluated by infecting mice with 1 x 10^4 cells. The parasitemia was counted daily till day 7. (**e**) A representative WT *T. b. brucei* and HpHbR-3'PAD1 cell isolated from the blood of mice; the latter ones internalized the fluorescently-labeled HpHb complex (green). (**f**) Based on morphology and the HpHb complex uptake, the same cells as in (e) were categorized as slender (SL) or stumpy (ST), the latter with the HpHb complex internalized (Hp-Alexa 488^+) or not (Hp-Alexa 488^-). All experiments above (n=3) were analyzed for significant differences using Student's *t*-test (ns, $p>0.05$; *, $p\leq0.05$; **, $p\leq0.01$; ****, $p\leq0.0001$). (**g**) The capacity to establish midgut infection in tsetse flies was determined for WT *T. b. brucei* and HpHbR-3'PAD1 cells isolated from the blood of mice. Bloodstream stage parasites were administrated in the fly's first bloodmeal without (-GSH) or with supplementation of 10 mM glutathione (+GSH).

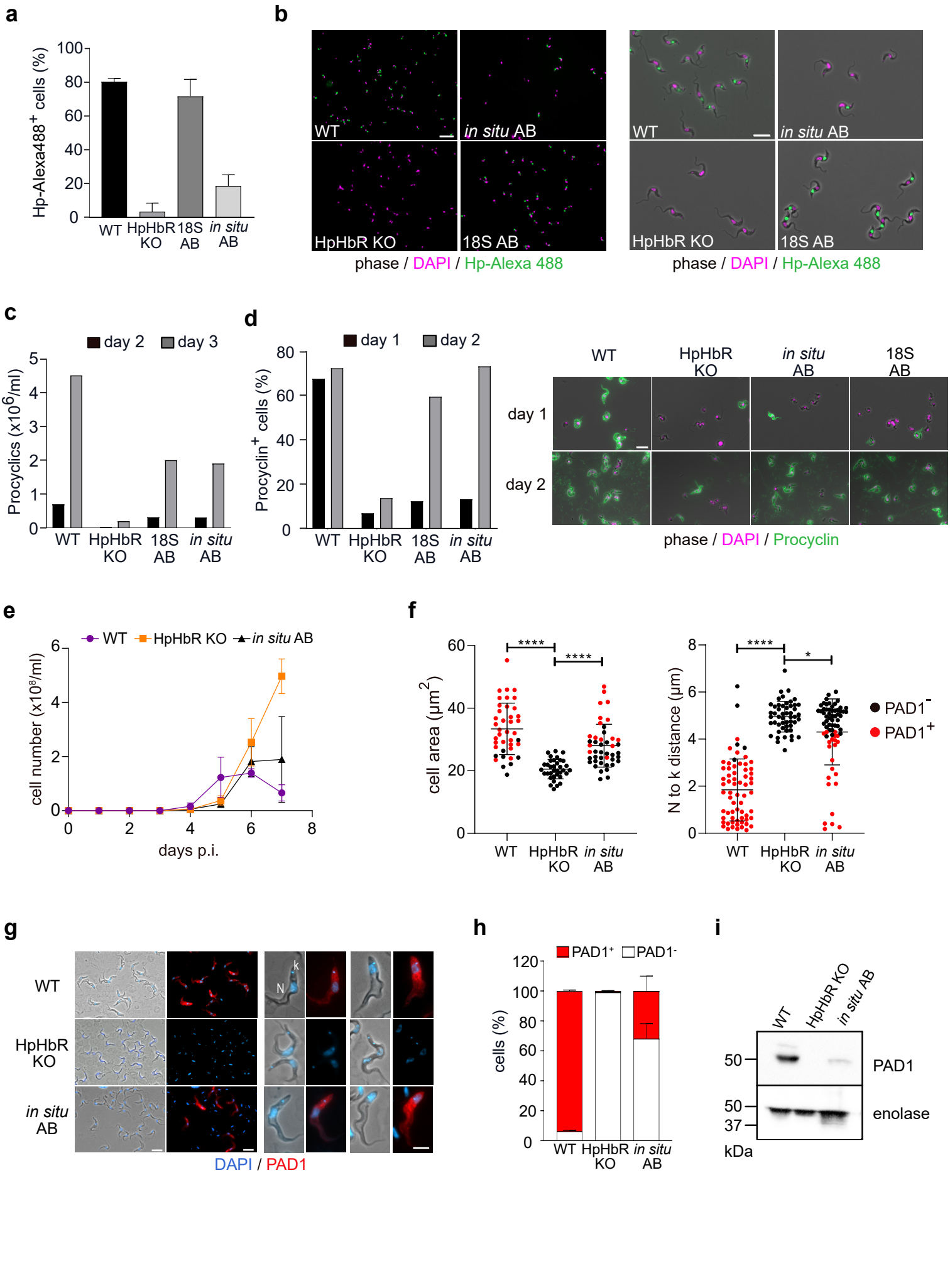
a
Hp-Alexa488+ cells (%)
100
80
60
40
20
0
WT
HpHbR KO
18S AB
in situ AB
b
WT
in situ AB
HpHbR KO
18S AB
phase / DAPI / Hp-Alexa 488
WT
in situ AB
HpHbR KO
18S AB
phase / DAPI / Hp-Alexa 488
c
day 2
day 3
Procyclics (x10^6/ml)
5
4
3
2
1
0
WT
HpHbR KO
18S AB
in situ AB
d
day 1
day 2
Procyclin+ cells (%)
80
60
40
20
0
WT
HpHbR KO
18S AB
in situ AB
WT
HpHbR KO
in situ AB
18S AB
day 1
day 2
phase / DAPI / Procyclin
e
WT
HpHbR KO
in situ AB
cell number (x10^6/ml)
6
4
2
0
0
2
4
6
8
days p.i.
f
cell area (µm^2)
60
40
20
0
****
****
WT
HpHbR KO
in situ AB
N to k distance (µm)
8
6
4
2
0
****
*
PAD1-
PAD1+
WT
HpHbR KO
in situ AB
g
WT
HpHbR KO
in situ AB
k
N
DAPI / PAD1
h
PAD1+
PAD1-
cells (%)
120
100
80
60
40
20
0
WT
HpHbR KO
in situ AB
i
WT
HpHbR KO
in situ AB
50
50
37
kDa
PAD1
enolase

Figure 4. Slender-to-stumpy form differentiation is disrupted in HpHbR knock-out cells

(**a**) The uptake of fluorescently-labeled haptoglobin (Hp) was monitored in WT *T. b. brucei*, HpHbR knock-outs (HpHbR KO), as well as in add-back cells, in which HpHbR was expressed either from the 18S rRNA locus (18S AB), or the *in situ* locus (*in situ* AB). All cells were harvested 4 days post-infection and mixed and incubated for 2 h with Hp-A488; (n=2) (**b**) Fluorescence microscopy of cell lines as in (a), with labeled Hp (green) and DNA visualized by DAPI (magenta). Note the absence of Hp uptake in HpHbR knock-outs. Left panel: Low magnification of the purified cells (scale bar, 20 μM); Right panel: Cells at higher magnification (scale bar, 10 μM). (**c**) *In vitro* differentiation of cell lines as in (a). Cells were placed to DTM medium with 3 mM sodium citrate/*cis*-aconitate at 27°C and procyclic cells were counted on day 2 and 3; (n=3) (**d**) Examination for procyclin expression on day1 and day 2 Left panel: Percentage of procyclin positive cells (procyclin^{+}) established by fluorescence microscopy with procyclin antibody (green) and DAPI (magenta). Right panel: Representative pictures for each cell line; (n=3) (**e**) *In vivo* infectivity of WT *T. b. brucei*, HpHbR KO, and the *in situ* AB was evaluated by infecting mice with 1 x 10^4 cells. The parasitemia was counted daily till day 7 when the experiment was terminated. Parasites from infections were harvested on day 7 post-infection and separated from blood using the DEAE column. (**f**) Morphological characterization of cell lines described in (e), containing the PAD1-positive ST forms (red dots) along with the PAD1-negative (SL) cells (black dots). Left panel: cell area; Right panel: the distance between the nucleus (N) and the kinetoplast (k). Results were analyzed for significant differences using Student's *t*-test (*, p≤0.05; ****, p≤0.0001). (**g**) Indirect immunofluorescence with PAD1 antibody (red), which is specific for ST Left panel: Low magnification of the purified cells (scale bar, 10 μM); Right panel: Individual cells at high magnification (scale bar, 5 μM), with discernible DAPI-stained nucleus (N) and kinetoplast (k). (**h**) Quantification of PAD1-positive and PAD1-negative cells (*ex vivo*, day 7 p.i.) described in (e). In the columns, the stumpy form is shown in red. (**i**) Western blot analysis with PAD1 antibody of cell lines described in (e). Enolase antibody was used as a loading control.

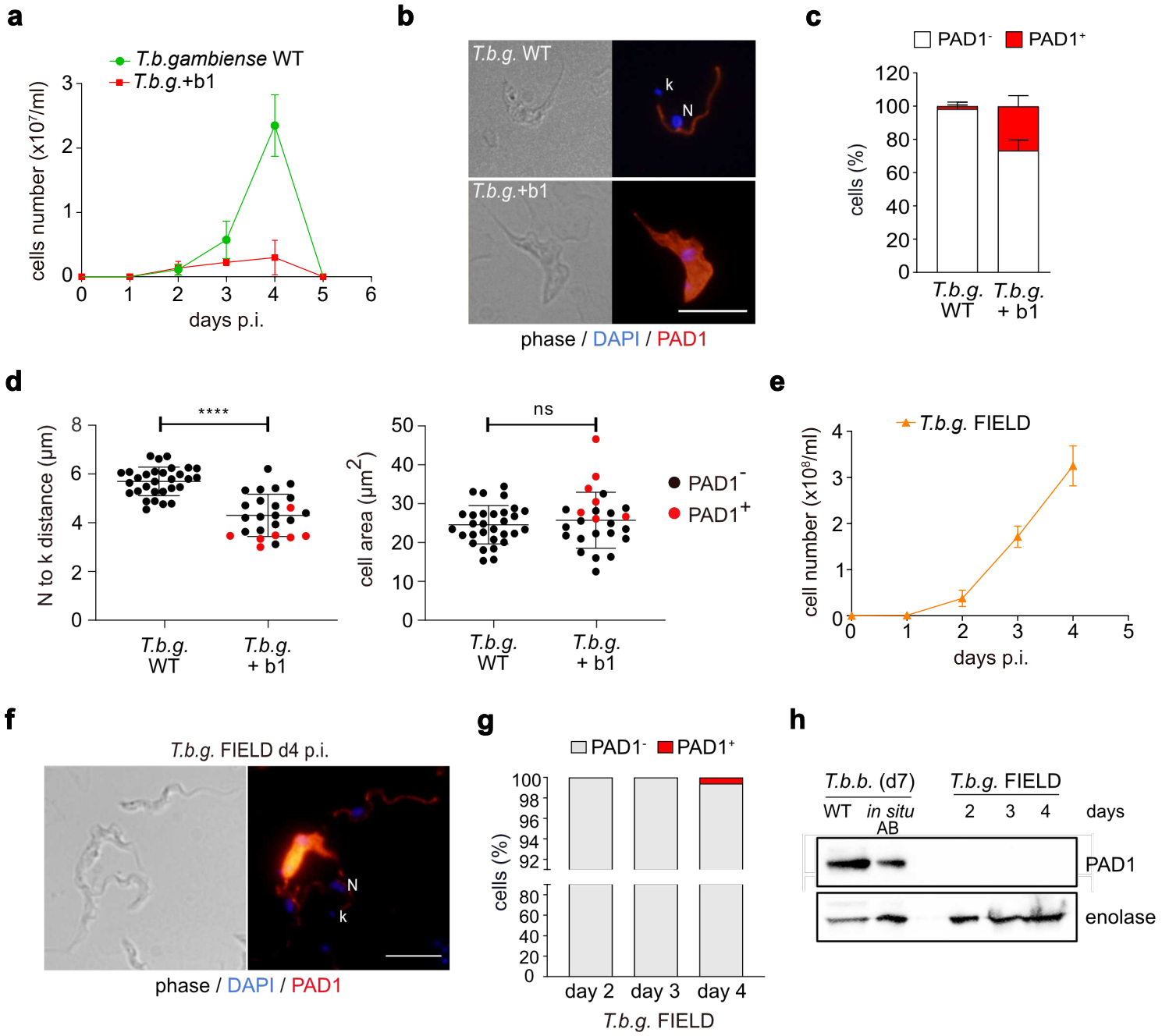

Figure 5. Restoration of stumpy formation in *T. b. gambiense*

(**a**) *In vivo* infectivity of WT *T. b. gambiense* LiTat 1.3 (green line) and *T. b. gambiense* expressing *T. b. brucei* HpHbR from the 18S rRNA locus (*T. b. g.* + b1) (red line) was evaluated by infecting mice with 3 x 10^6 cells; n=3. The parasitemia´was counted daily till day 6, when the experiment was terminated. (**b**) Indirect immunofluorescence with PAD1 antibody (red), which is specific for ST. DNA in the nucleus (N) and kinetoplast (k) was stained with DAPI (blue). Scale bar, 5 µm. (**c**) Quantification of PAD1-positive and PAD1-negative cells (*ex vivo*, day 4 p.i.) described in (a); (n=3). In the columns, the stumpy form is shown in red. (**d**) Morphological characterization of cell lines described in (a), containing the PAD1-negative cells (black dots) or PAD1-positive cells (red dots). Left panel: the distance between the nucleus (N) and the kinetoplast (k); Right panel: cell area. Results were analyzed for significant differences using Student's *t*-test (ns, p0.05; ****, p≤0.0001). (**e**) *In vivo* infectivity of *T. b. gambiense* Bosendja Field strain. The parasitemia was counted daily till day 4, when the experiment was terminated.; (n=3) (**f**) Immunofluorescence using PAD1 antibody, which reveals a fraction of the PAD1-positive cells. DNA in the nucleus (N) and kinetoplast (k) was stained with DAPI (blue). Scale bar, 5 µm. (**g**) Quantification of PAD1-positive and PAD1-negative cells in the *T. b. gambiense* Field strain *ex vivo* days 2-4 p.i. (**h**) PAD1 antibody Western blot analysis of WT *T. b. brucei* and *in situ* AB, as well as *T. b. gambiense* Field strain. Enolase antibody was used as a loading control.

Figures

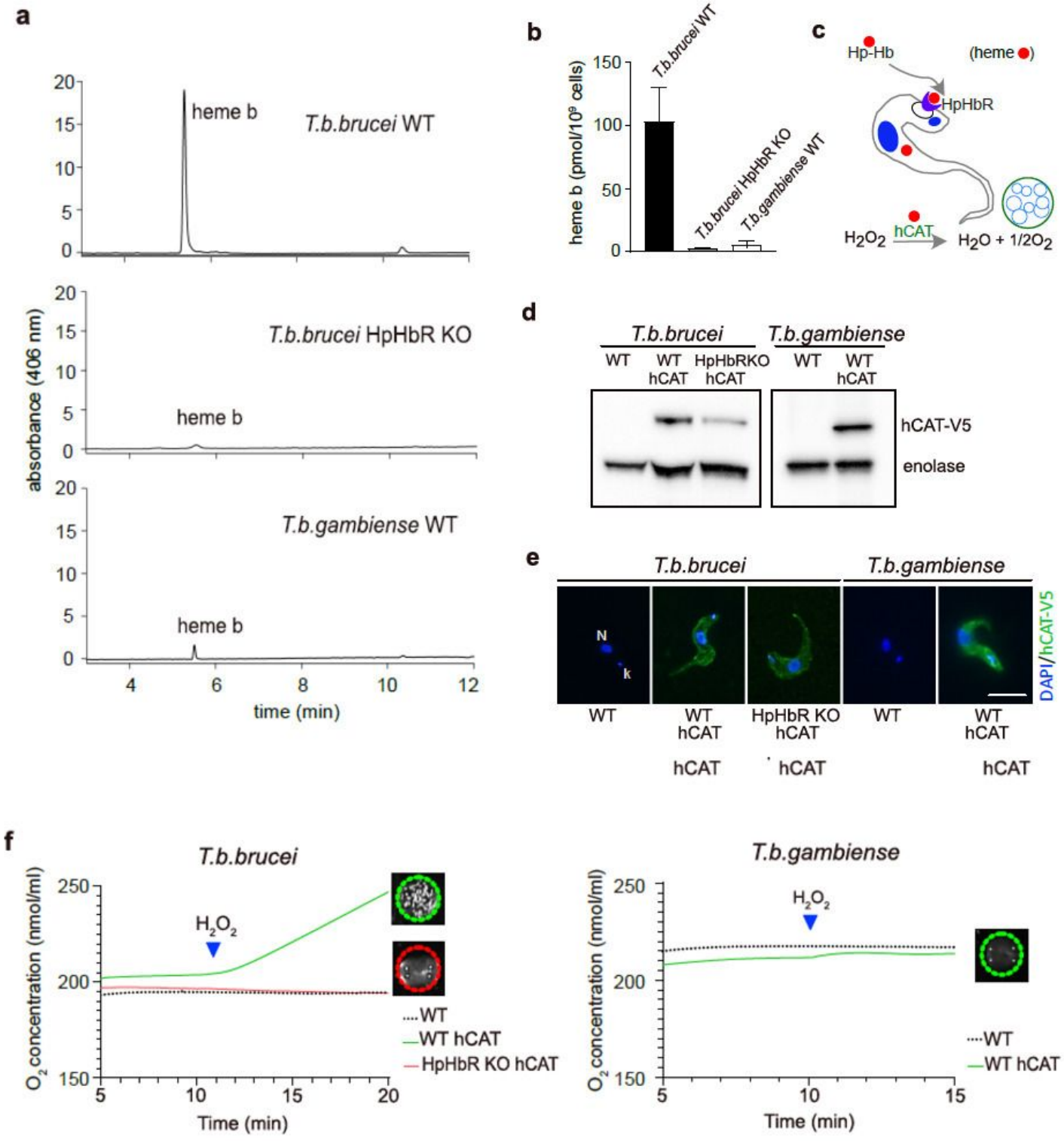

Figure 1

Detection of heme and hemoproteins in bloodstream stages of T. b.brucei and T. b. gambiense

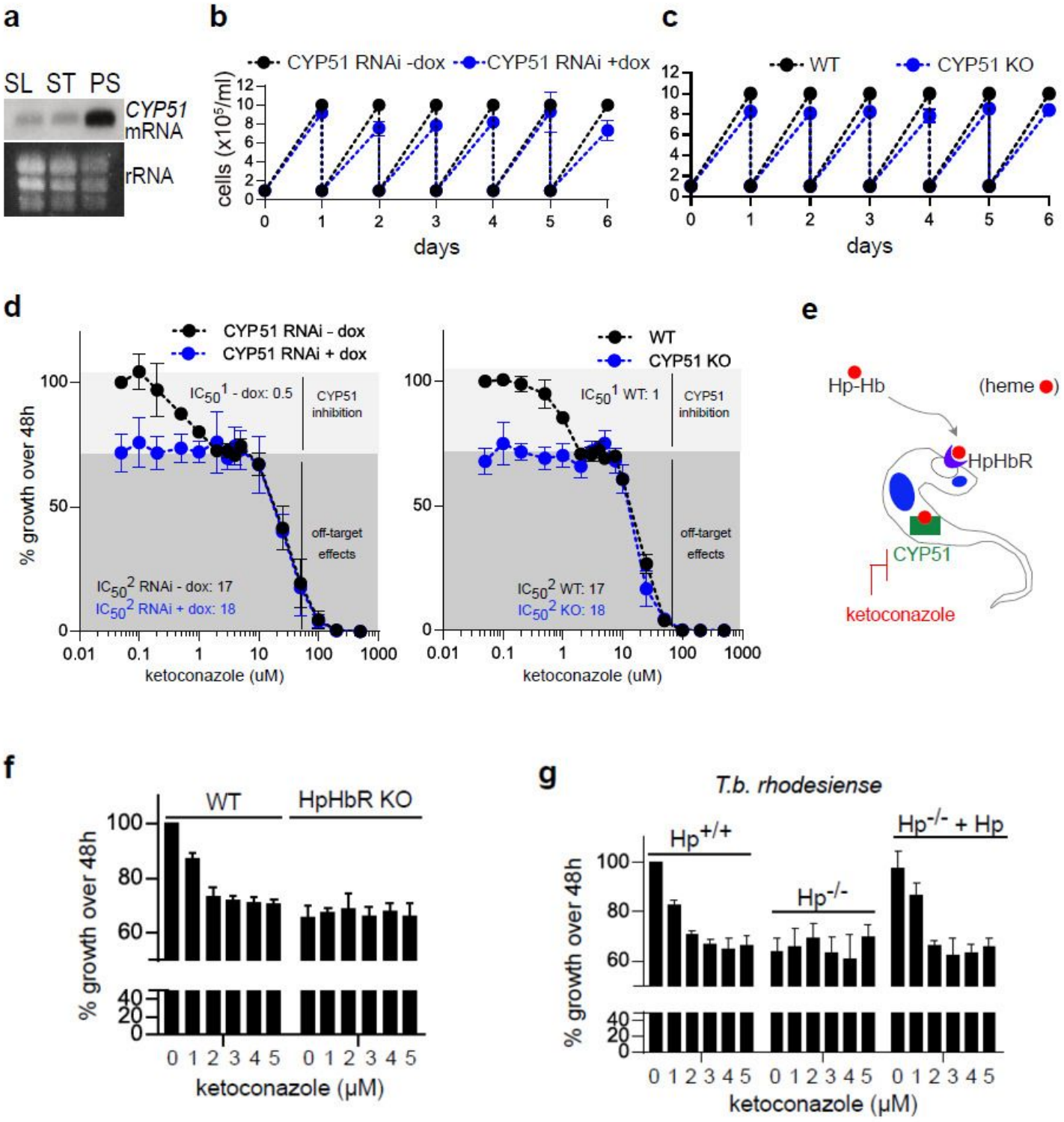

Figure 2

Effect on growth and ketoconazole sensitivity after CYP51 invalidation in the bloodstream stage

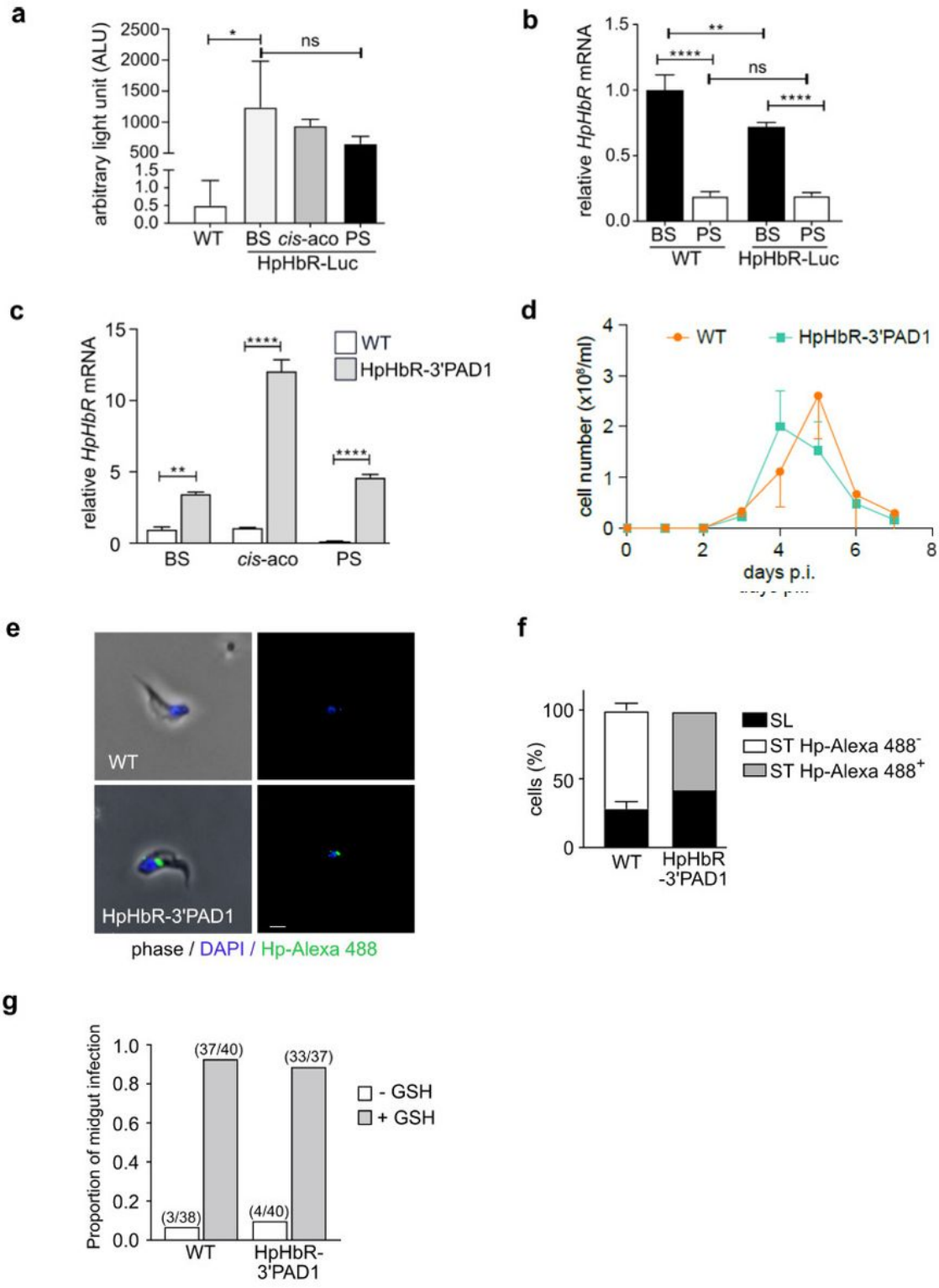

Figure 3

Artificial expression of HpHbR in stumpy form does not interfere with life cycle progression

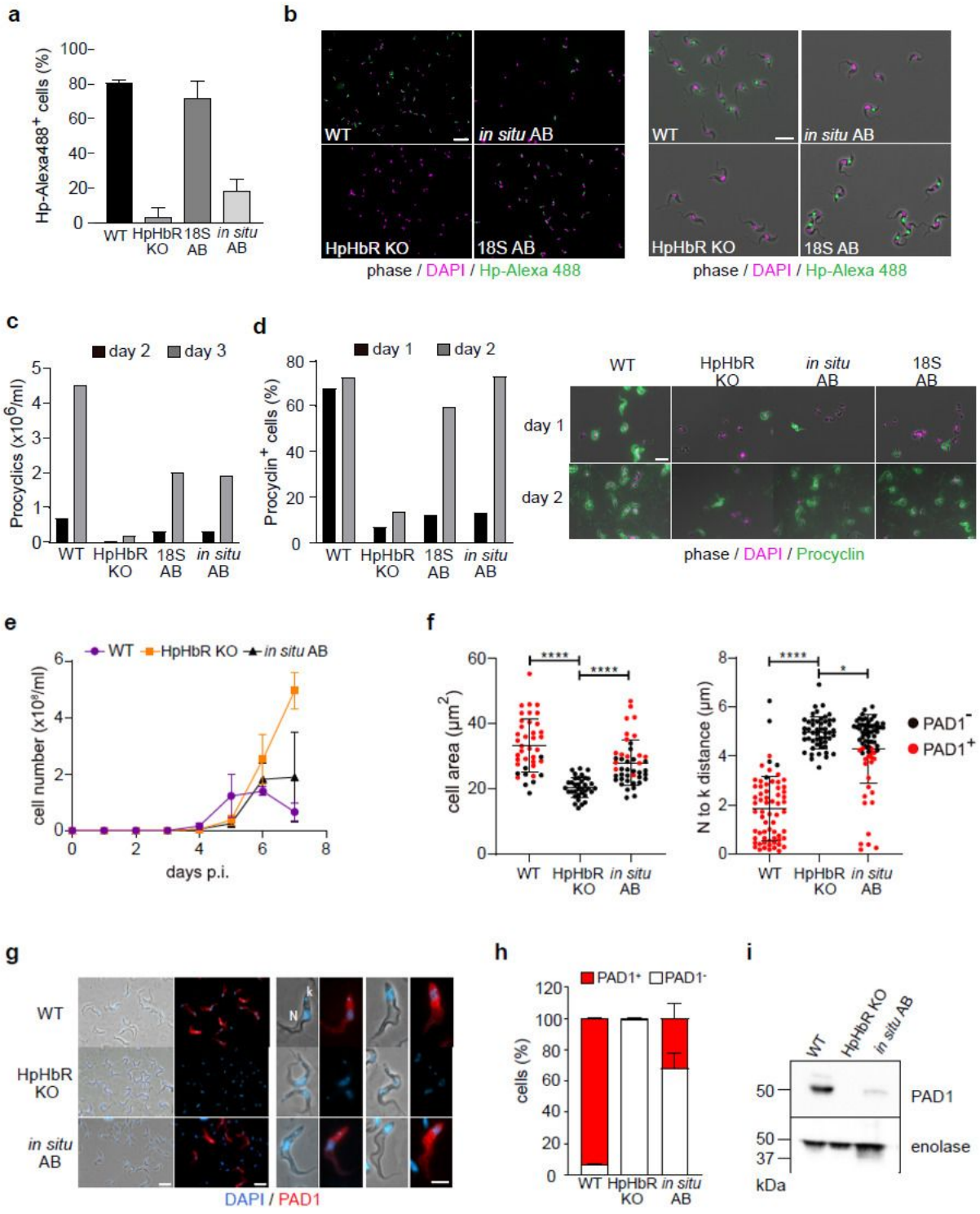

Figure 4

Slender-to-stumpy form differentiation is disrupted in HpHbR knock-out cells

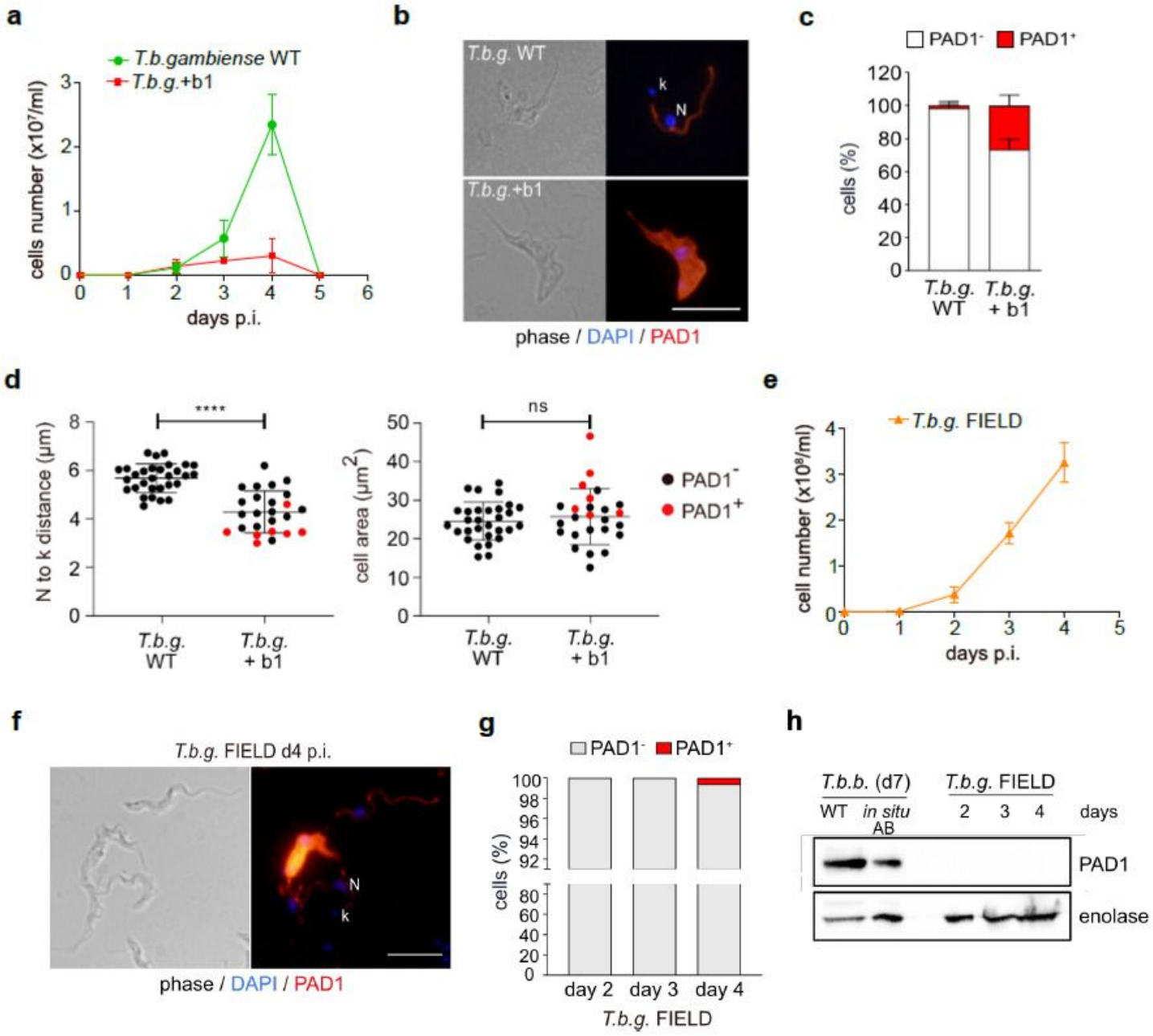

Figure 5

Restoration of stumpy formation in T. b.gambiense (a) In vivo infectivity ofWT T. b.gambiense LiTat1.3(greenline)and

Supplementary Files

This is a list of supplementary files associated with this preprint. Click to download.

- HorakovaHpHbRSupplementary.pdf